

The radio emission from the Galaxy at 22 MHz

R.S. Roger¹, C.H. Costain^{*,1}, T.L. Landecker¹, and C.M. Swerdlyk^{1,2}

¹ National Research Council Canada, Herzberg Institute of Astrophysics, Dominion Radio Astrophysical Observatory, Penticton, B.C. Canada V2A 6K3

e-mail: robert.roger@hia.nrc.ca

² Now at University of Victoria, Victoria, B.C., Canada

Received October 22, 1998; accepted January 4, 1999

Abstract. We present maps of the 22 MHz radio emission between declinations -28° and $+80^\circ$, covering $\sim 73\%$ of the sky, derived from observations with the 22 MHz radiotelescope at the Dominion Radio Astrophysical Observatory (DRAO). The resolution of the telescope (EW \times NS) is $1.1^\circ \times 1.7^\circ \sec(\text{zenith angle})$. The maps show the large scale features of the emission from the Galaxy including the thick non-thermal disk, the North Polar Spur (NPS) and absorption due to discrete H II regions and to an extended band of thermal electrons within 40° of the Galactic centre. We give the flux densities of nine extended supernova remnants shown on the maps. A comparison of the maps with the 408-MHz survey of Haslam et al. (1982) shows a remarkable uniformity of spectral index ($T \propto \nu^{-\beta}$) of most of the Galactic emission, with β in the range 2.40 to 2.55. Emission from the outer rim of the NPS shows a slightly greater spectral index than the distributed emission on either side of the feature. The mean local synchrotron emissivity at 22 MHz deduced from the emission toward nearby extended opaque H II regions is $\sim 1.5 \cdot 10^{-40} \text{ Wm}^{-3} \text{ Hz}^{-1} \text{ sr}^{-1}$, somewhat greater than previous estimates.

Key words: Galaxy: structure — radio continuum: general; ISM

1. Introduction

The nonthermal radio continuum emission from the Galaxy at frequencies below 100 MHz is the synchrotron radiation of cosmic ray electrons with energies of order 1 GeV. Measurements of the emissivity and the spectral index of the emission provide direct information about the electron energy spectrum and the magnetic field strength

in the Galaxy. At frequencies below about 40 MHz, the opacity of the thermal component of Galactic emission is often sufficient to absorb the much brighter background synchrotron emission, providing a means of estimating local synchrotron emissivities in the directions of H II regions at known distances.

There have been numerous surveys made of Galactic emission below 500 MHz including: the all-sky map of Haslam et al. (1982) at 408 MHz; the northern sky maps of Turtle & Baldwin (1962: 178 MHz, -5° to $+90^\circ$), of Milogradov-Turin & Smith (1973: 38 MHz, -25° to $+70^\circ$) and of Caswell (1976: 10 MHz, -6° to $+74^\circ$, 0^h to 16^h); and southern sky maps of Landecker & Wielebinski (1970: 150 MHz and 85 MHz, -15° to $+15^\circ$), Hamilton & Haynes (1969: 153 MHz, $+5^\circ$ to -90°), Alvarez et al. (1987: 45 MHz, $+19^\circ$ to -90°), and Ellis (1982: 16.5 MHz, 0° to -90°).

The 22 MHz Telescope at the DRAO was used in the period 1965 to 1969 to measure the emission from discrete sources and to map the background radiation from our galaxy. The telescope has been described completely by Costain et al. (1969); only those details relevant to the present paper are given here. Flux densities of point sources have been published by Roger et al. (1969) and by Roger et al. (1986). The low-frequency spectra of these sources have been discussed by Roger et al. (1973). Technical problems prevented a satisfactory calibration of the Galactic emission, but these problems have now been circumvented and in this paper we present a map of the Galactic emission at 22 MHz between declinations -28° and $+80^\circ$ covering the complete range of right ascension, $\sim 73\%$ of the sky. By comparing the 22 MHz map with the 408 MHz data from the all-sky survey of Haslam et al. (1982) we have prepared a map of the spectral index of the emission over the same area. We also derive values of the local synchrotron emissivity.

Send offprint requests to: R.S. Roger

* Deceased December, 1989.

2. The telescope

The telescope was an unfilled aperture in the form of a T with dimensions $96\lambda \times 2.5\lambda$ east-west (EW) and $32.5\lambda \times 4\lambda$ north-south (NS). This array formed a nearly Gaussian beam of extent 1.1×1.7 degrees (EW \times NS) at the zenith (declination 48.8°). The telescope was operated as a meridian transit instrument, steerable in declination between -30° and the North Celestial Pole by the adjustment of the phases of rows of dipole elements in the north-south direction. Away from the zenith, foreshortening of the array broadened the beam in this direction to $1.7^\circ \sec(Z)$, where Z is the zenith angle. The gain of the telescope in directions away from the zenith was further reduced by the response of the basic array element, a full-wave dipole $\frac{\lambda}{8}$ above a reflecting screen. Aperture grading by means of attenuators was used to keep side-lobes to a level of a few percent.

The pencil-beam response was formed by multiplying the signals from the EW and NS arms. A problem in T - and cross-format telescopes arises from the region in which the two arms intersect. If this region is removed, a broad negative response is produced around the narrow pencil beam, and the telescope filters out the lowest spatial frequencies, leading to a poor representation of the broadest angular components of the emission. To overcome this problem, the signals from the elements in the overlap region were split and fed to both the EW and NS arrays.

The gain of the antenna (in effect the ratio between the flux density of a radio source and the antenna temperature it produces in the main beam) was established using an assumed flux density of 29100 ± 1500 Jy for Cygnus A. Details of the original flux-density scale and the subsequent revision can be found in Roger et al. (1973) and in Roger et al. (1986).

3. Observations and basic data reduction

Observations were made in several modes during the working life of the telescope. In the early part of the observation period the telescope formed only one beam which could be moved in declination by operating the NS phasing switches. Long scans at fixed declination were made to observe the background emission as well as point sources, and short scans were made to measure the flux density of point sources with the beam switched frequently between different declinations. Only the scans of long duration were used to assemble the data presented in this paper. At a later stage, more automated phasing switches were added to permit rapid time-shared observations at five adjacent declinations. A large fraction of the present data was obtained from long scans with this equipment.

Scans were made at a set of standard declinations, chosen to sample the emission at half-beamwidth intervals.

Since the NS beamwidth increased with increasing zenith angle, the standard declinations were not evenly spaced.

The observations were made mostly in the years 1965 to 1969 which covered a period of fairly low solar activity. Nevertheless, because of the low frequency of operation, the influence of the ionosphere on the observations was often large. Observations of point sources were affected by refraction, scintillation, and absorption in differing degrees. A correction factor for ionospheric absorption (primarily a daytime phenomenon) was derived from an on-site 22 MHz riometer and was applied to the data. Refraction amounting to a significant fraction of the (EW) beam was detected only near times of sunrise in the ionosphere when large horizontal gradients of electron density were present. Scintillation of "point sources" (sources less than $15'$ diameter) was a frequent occurrence. Due to lack of correlation of the phase and amplitude variations over the extent of the telescope array during times of severe scintillation, flux densities could be seriously underestimated. To overcome this problem, many observations of each source were made and measurements of flux density were derived from only those observations judged to be the least affected. By contrast, most observations of the extended emission were largely unaffected by scintillation and, after correction for absorption, could be reliably averaged together. The data presented here are the result of averaging at least two observations, and in many parts of the sky up to five good observations contributed to the average.

Thus, the basic data set is a data array assembled from the averaged scans at the standard declinations. Because neighbouring averaged scans contained data observed at different times with varying conditions, the array displayed significant scanning artifacts. These were greatly reduced by the application of a Fourier filtering process in the declination dimension. The data were then interpolated onto a grid sampled at 1 minute intervals in right ascension and $15'$ in declination.

4. Further data processing

Comparison of the resulting map with maps at higher frequencies suggested that the brightness temperature calibration of the 22 MHz map had a zenith-angle-dependent error. We used the 408 MHz all-sky survey of Haslam et al. (1982) for comparisons because these single-paraboloid observations would likely be free of such defects, but comparisons with other similar data sets would probably have produced similar conclusions.

For comparison with the 22 MHz map we convolved the 408 MHz data from its original resolution of $51'$ to the variable beamwidth of our data. Calculation of a map of spectral index between the two frequencies indicated a systematic variation of spectral index with declination. Since such an effect is unlikely to be real, we suspected a calibration problem in the 22 MHz data. Although the cause

is not fully understood, we believe that the response of the telescope to extended structure differed from its response to point sources in directions away from the zenith. This effect is discussed in Sect. 6.2. We believe, however, that the response of the telescope at the zenith (declination 48.8°) is well understood. At this declination, we plotted brightness temperature at 22 MHz against brightness temperature at 408 MHz (a $T-T$ plot). We used data at all right ascensions except (a) near the Galactic plane in the Cygnus region (at $\sim 21^{\text{h}}$, 48°) where strong absorption features are evident in the 22 MHz map (see below) and (b) regions around a few strong small-diameter sources. Figure 1 shows this plot. The highest temperatures in Fig. 1 correspond to the Galactic plane in the anticentre (at $4^{\text{h}} 40^{\text{m}}$, 48°) where there may be a small amount of absorption, causing the $T-T$ plot to deviate from a straight line. Using all the data shown in Fig. 1 we derived a differential spectral index of $2.52 \pm .02$. Restricting the fit to regions with $T_{22} < 50$ kK (corresponding to right ascensions between $5^{\text{h}} 40^{\text{m}}$ and $18^{\text{h}} 10^{\text{m}}$) the correlation is very tight and the differential spectral index is $2.57 \pm .02$. These values of spectral index are close to the value expected in this frequency range from the work of Bridle (1967) and Sironi (1974) indicating that the temperature scale at 22 MHz is accurate. Furthermore, the extrapolation of the line fitted to the data points passes close to the origin of the $T-T$ plot, giving us confidence that the zero level of the 22 MHz measurements is also well established at the zenith. $T-T$ plot analyses at other declinations (again excluding areas of absorption) indicate that the zero level is acceptably correct throughout the declination range, but that the temperature scale varies (the accuracy of the zero level is discussed in Sect. 6.1).

The temperature scale at declinations away from the zenith was adjusted using the following procedure. At each declination the average brightness temperature ratio between 22 MHz and 408 MHz was calculated (using $T-T$ plots) over the range 8 to 16 hours in right ascension (to exclude extended absorption regions on the Galactic plane). The temperature scale at 22 MHz was then adjusted to make this ratio equal to that at the zenith (note that Fig. 1 shows data over a wider range of right ascension).

In order to cover the central regions of the Galaxy, we have included observations as far south as declination -28° , where the telescope was operating at a zenith angle of 76.8° . At these large zenith angles, there is some departure of the antenna gain function from its calculated value (see Costain et al. 1969). However, reliable flux densities of point sources have been obtained as far south as declination -17.4° (Roger et al. 1986) and we believe that our calibration procedure remains reasonably effective to the southern limit of our map.

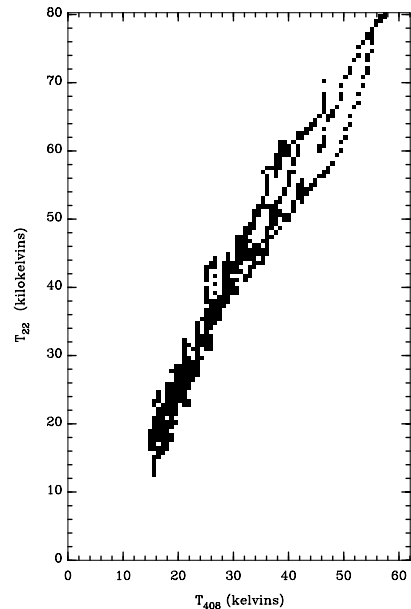


Fig. 1. A $T-T$ plot of 22 MHz and 408 MHz data for declination 48.8° and all right ascensions except a) for the range 20^{h} to 22^{h} and b) small regions around bright point sources

5. Results

5.1. Map of the northern sky at 22 MHz

Figure 2 shows in equatorial coordinates a contoured grayscale map of the 22 MHz emission from the sky between declinations -28° and 80° in five segments. Figure 3 depicts the data between Galactic latitudes -40° and $+40^\circ$ with the same contours and grayscale in Galactic coordinates, and with positions of extended Galactic sources indicated. Figure 4 is a grayscale representation of the full data set in Aitoff projection of Galactic coordinates.

The brightness temperature of the 22 MHz emission varies from ~ 17 kK towards a broad minimum about 50° off the Galactic plane at the longitude of the anticentre to over 250 kK on the plane near the Galactic centre. The brightness temperature near both north and south Galactic poles is approximately 27 kK. The Galactic plane itself is apparent over the full range of longitude from $+1^\circ$ to $+244^\circ$. At various points along the plane, particularly at lesser longitudes, depressions are apparent in the emission. These represent thermal free-free absorption of bright synchrotron background emission by relatively nearby, opaque regions of dense ionized gas.

Two other large-scale features apparent in the maps are Loop I, the North Polar Spur (NPS), rising from the plane near longitude 30° , and Loop III, centred near longitude 87° .

We emphasize that the main value of the data lies in the representation of structure larger than the beam. The strongest point sources (Cas A, Cyg A, Tau A and Vir A) have been removed from the map. While other

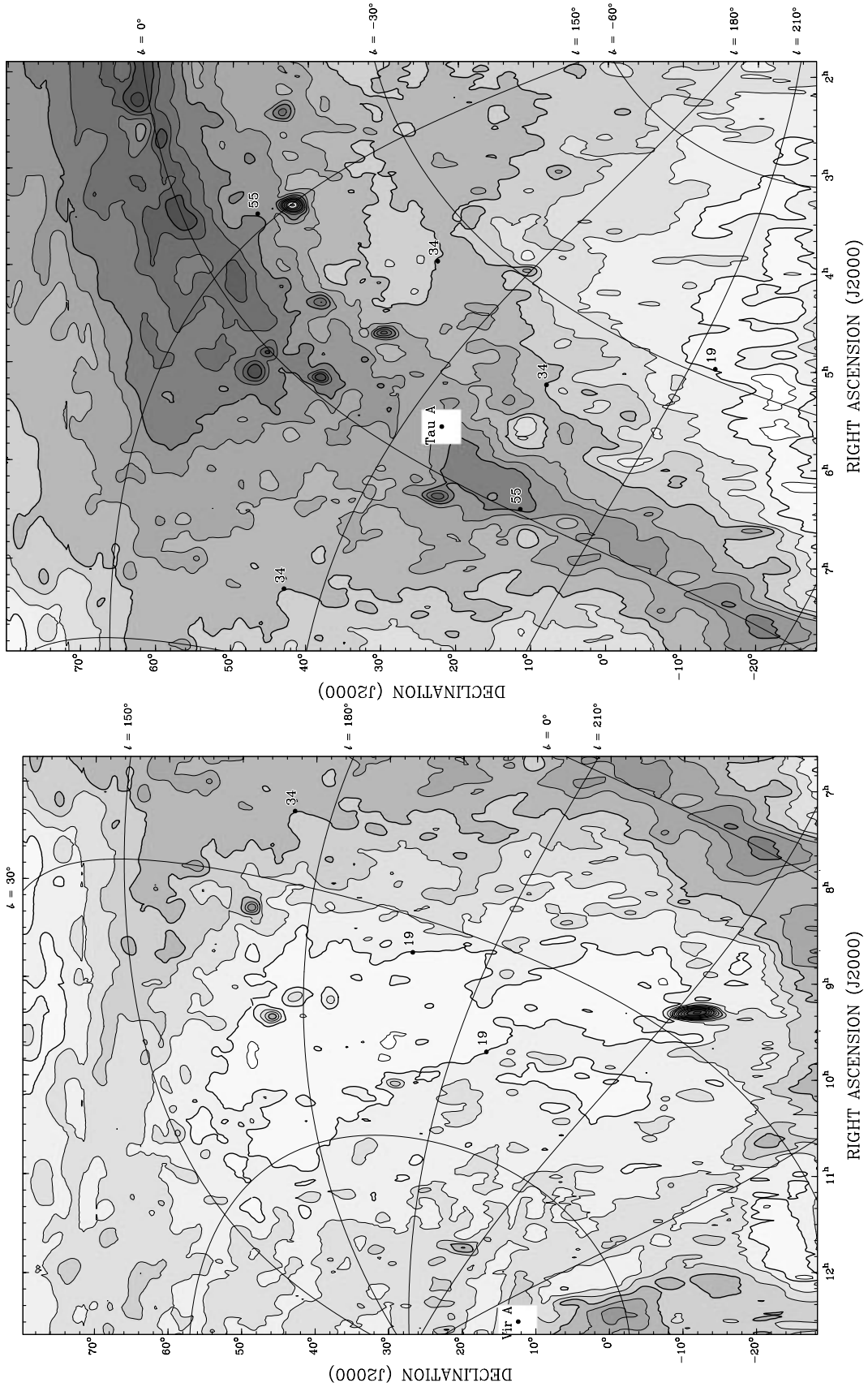


Fig. 2. A map of the emission at 22 MHz. Contours of brightness temperature are at the following levels in kilokelvins: 14, 19, 24, 29, 34, 41, 48, 55, 65, 75, 85, 100, 115, 130, 150, 170, 190, 220, 250. Levels in bold have thick contour lines and are labelled. Regions affected by sidelobes of four strong sources are blanked out. The superimposed grid shows Galactic co-ordinates in steps of 30° in l and b , labelled only where grid lines intersect the right-hand side and the top of the figure

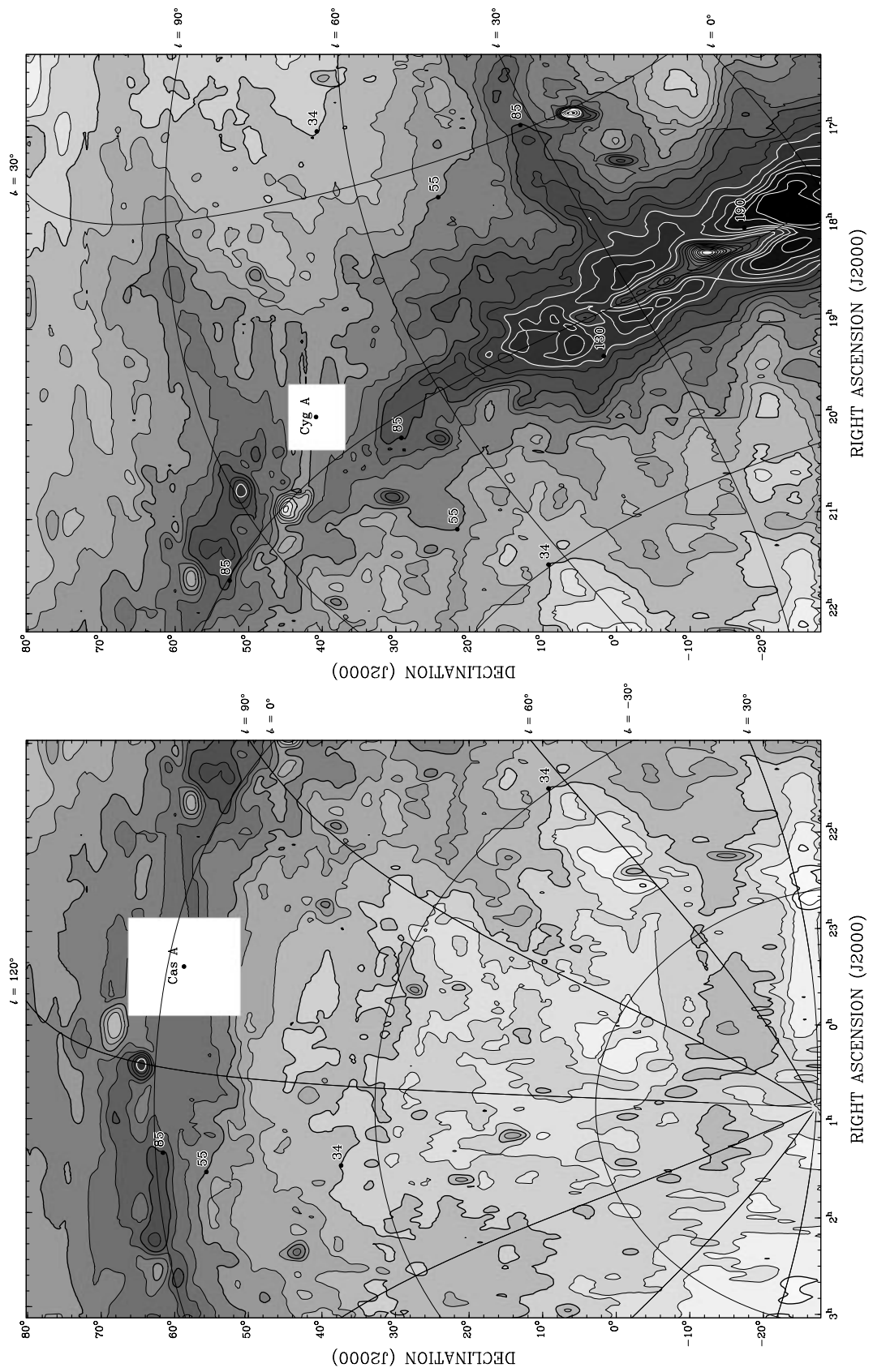


Fig. 2. continued

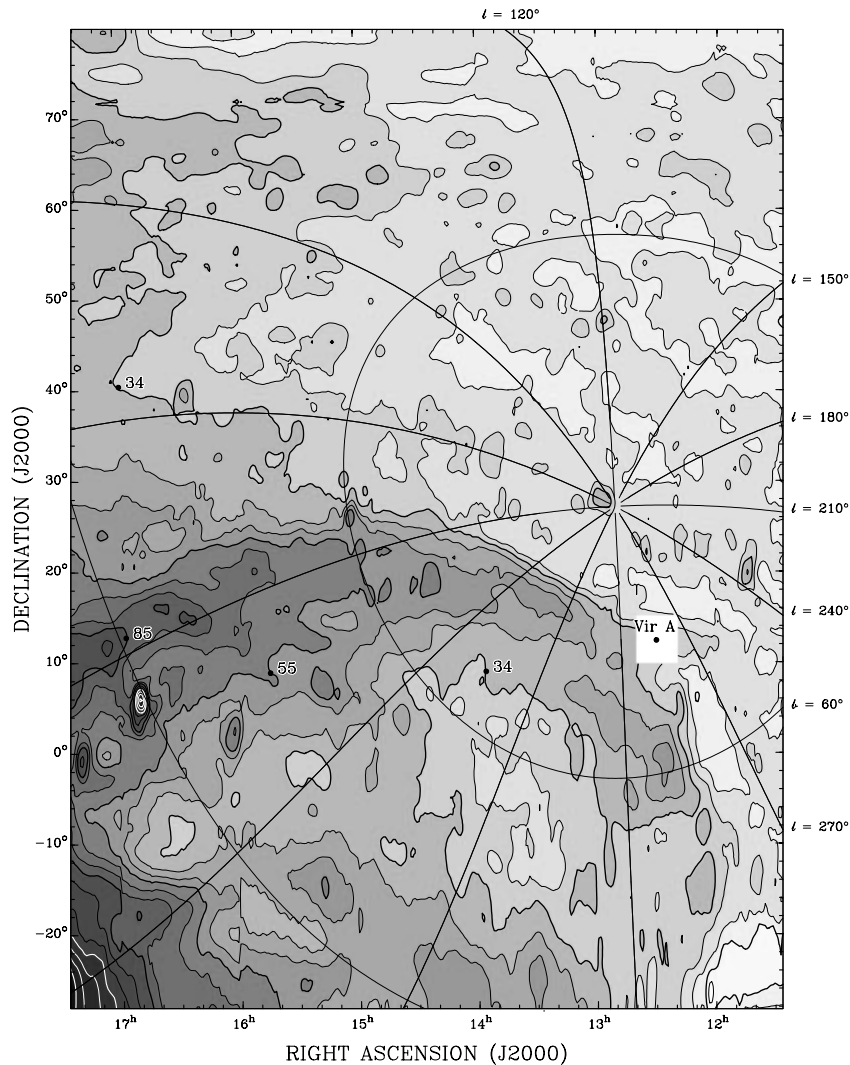


Fig. 2. continued

point sources remain in the maps, these data cannot be used to determine their flux densities. First, the ionospheric effects mentioned above cause the point sources to be very poorly represented in these maps. Second, the scaling applied after comparison with the 408 MHz data will have further affected the flux densities of point sources at declinations away from the zenith. Reliable point source flux densities are already available in the published lists referred to in Sect. 1.

5.2. Extended Galactic sources – supernova remnants

A number of extended supernova remnants are apparent in the data and the positions of these are indicated with labels in Fig. 3. The flux densities of most of the SNRs have been previously measured from the original observations and published in various papers. We have collected these and listed them in Table 1 together with new flux densities for two additional remnants not previously

reported. One other SNR, HB21, is indicated in Fig. 3 but *not* listed in Table 1 because of difficulties in separating its emission from that of nearby confusing sources.

5.3. Absorption of the background emission – H II regions

Depressions in the background emission near the Galactic plane are identified with a number of extended H II regions, which at frequencies near 20 MHz will largely obscure background emission. We list the properties of 21 of these discrete absorption regions in Table 2, with positions plotted in Fig. 3.

Figures 2, 3 and particularly 4 show the extended trough of absorption between $l = 10^\circ$ and $l = 40^\circ$. This trough undoubtedly extends to and past the Galactic centre but the increasingly extended N–S width of the telescope beam at large zenith angles was unable to fully resolve the feature below $l = 10^\circ$.

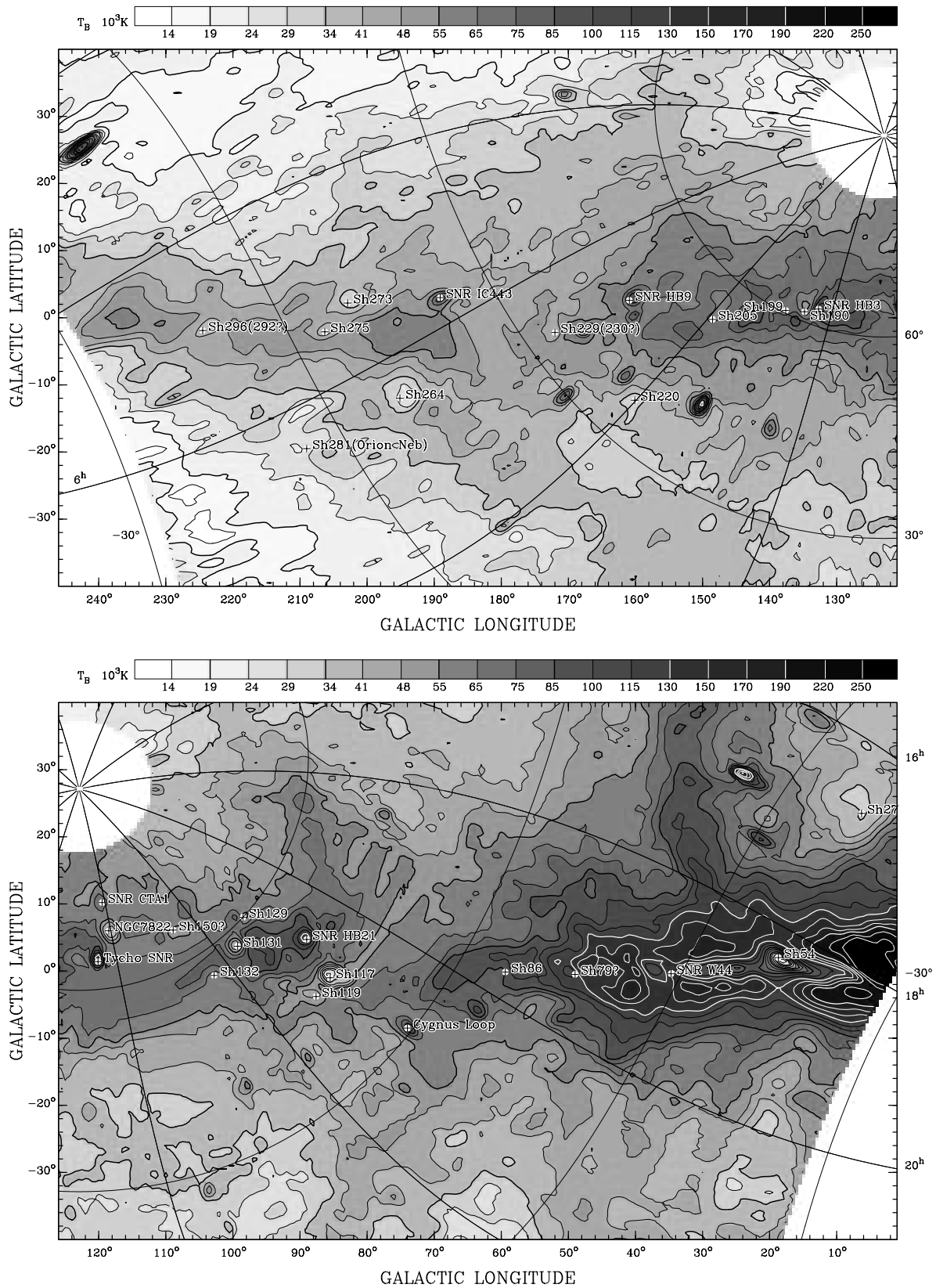


Fig. 3. The 22 MHz emission in Galactic coordinates in two segments with positions of prominent Galactic sources indicated. Contours, at the same levels shown in Fig. 2, are indicated with a bar scale. The superimposed grid shows equatorial co-ordinates (J2000) in steps of 2^h in right ascension and 30° in declination

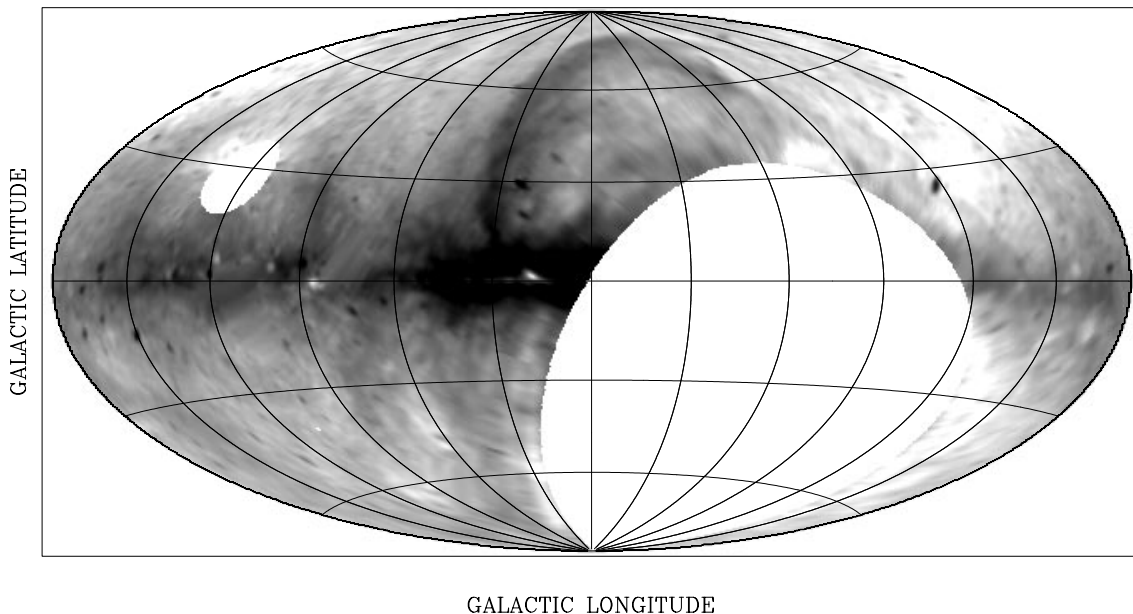


Fig. 4. An Aitoff projection of the 22 MHz emission in Galactic coordinates. The Galactic centre is at the map centre and grids are at 30° intervals in longitude and latitude, positive to the left and upwards respectively. Note the arc of the North Polar Spur rising from the plane near longitude $+30^\circ$

Table 1. Flux densities of supernova remnants at 22 MHz

SNR	Designation	Flux density Jy	Reference
$G34.7 - 0.4$	W44, 3C 392	881 ± 108	Roger et al. (1986)
$G74.0 - 8.5$	Cygnus Loop	1378 ± 400	this paper
$G93.3 + 6.9$	DA530, 4C(T)55.38.1	74 ± 20	Roger & Costain (1976)
$G119.5 + 10.2$	CTA1	632 ± 200	Pineault et al. (1997)
$G120.1 + 1.4$	3C10, Tycho SN1572	680 ± 54	Roger et al. (1986)
$G132.7 + 1.3$	HB3	450 ± 70	Landecker et al. (1987)
$G160.9 + 2.6$	HB9	1130 ± 340	this paper
$G184.6 - 5.8$	Crab Nebula, SN1054	3160 ± 380	Roger et al. (1986)
$G189.1 + 3.0$	IC 443, 3C 157	615 ± 75	Roger et al. (1986)

5.4. The spectral index of emission, 22 to 408 MHz

Figure 5 shows a map of spectral index calculated from the final 22 MHz map and the 408 MHz map (Haslam et al. 1982), the latter convolved to the declination-dependent beamwidth of the 22 MHz telescope. The spectral index, β , as displayed, is related to the brightness temperatures at each frequency, T_{22} and T_{408} , by the expression

$$\beta = \log(T_{22}/T_{408})/\log(408/22).$$

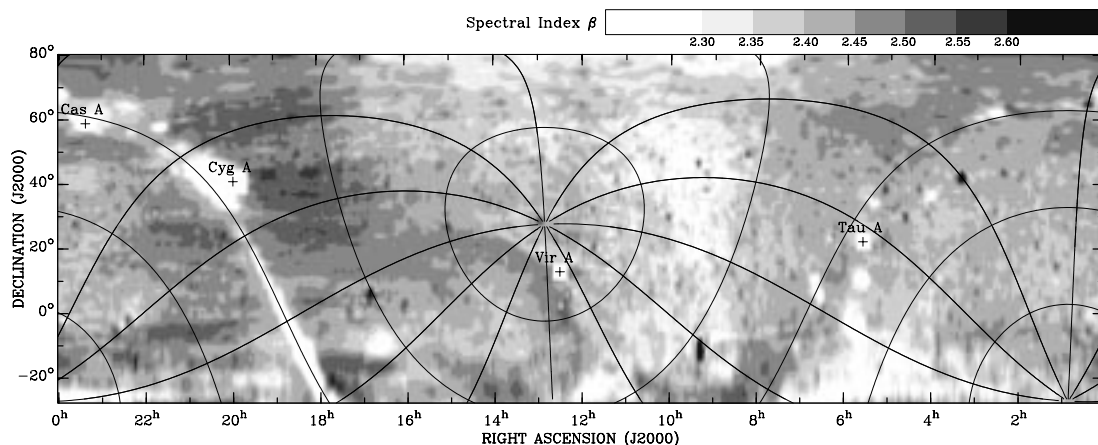
Because the 408 MHz map has been used to establish the variation of the 22 MHz temperature scale with declination, great care is needed in interpreting this map. The process of revising the 22 MHz scale could eliminate or reduce spectral index features between 8 and 16 hours right ascension with structure in the declination direction if they extend over a large range in this dimension. On the other hand, features in the spectral index map which have structure in the right ascension dimension are

likely to be largely unaffected by the correction process. Similarly, spectral index features with structure in various directions, including most features which have counterparts in the individual maps, would be suspect only if distortions appeared in the declination dimension. No such artefacts are apparent. However, some “banding” in declination, particularly below -3° , can be seen in specific right ascension ranges. This effect is easily recognized as spurious and is probably related to zero level errors in the 22 MHz or, possibly, in the 408 MHz map. Such effects may be aggravated by the large zenith angles at which these low-declination regions were observed at 22 MHz.

Errors in the spectral index map can arise from zero-level or temperature-scale errors at either frequency. We deal with zero-level errors first. Taking 5 kK as a possible error in the 22 MHz data (see the detailed discussion in Sect. 6.1) we estimate the effects on the spectral index map. The large frequency separation between 22.25 and 408 MHz means that zero-level errors have relatively

Table 2. H II regions in absorption

Galactic Coordinates	Region	Other Designation	Sharpless diameter
6.3 + 23.5	Sh 27	ζ -Oph	480'
18.7 + 2.0	Sh 54	II Ser, NGC 6604	140'
49.0 - 0.5	Sh 79(?)		40'
59.4 - 0.1	Sh 86	I Vul, NGC 6820	40'
85.5 - 1.0	Sh 117	NGC 7000	240'
87.6 - 3.8	Sh 119		160'
98.5 + 8.0	Sh 129	I Cep	140'
99.3 + 3.7	Sh 131	I Cep, IC 1396	170'
102.8 - 0.7	Sh 132	II Cep	90'
108.9 + 6.1	Sh 150(?)		40'
118.5 + 6.0	NGC 7822	IV Cep, Sh 171(?)	180'
134.8 + 0.9	Sh 190	IC 1805, W4	150'
137.6 + 1.1	Sh 199	IC 1848, W5	120'
148.5 - 0.2	Sh 205	I Cam	120'
160.1 - 12.3	Sh 220	NGC 1499, II Per	320'
172.0 - 2.2	Sh 229 (230?)	IC 405, (I Aur ?)	65'(300')
195.1 - 12.0	Sh 264	λ -Ori	390'
202.9 + 2.2	Sh 273	NGC 2264	250'
206.3 - 2.1	Sh 275	I Mon, NGC 2244	100'
209.0 - 19.5	Sh 281	Orion Neb, NGC 1976	60'
224.5 - 1.9	Sh 296 (292?)	(IC 2177?)	200'(21')

**Fig. 5.** A map of the spectral index from 22 MHz to 408 MHz in shaded grey levels as indicated by the bar scale. Regions near four strong sources are blanked out. The superimposed grid shows Galactic co-ordinates in steps of 30° in l and b

little effect: the ± 5 kK error will change spectral index by ± 0.1 at the sky minimum and by ± 0.01 on the brightest part of the Galactic plane. We tested the effect of an error of ± 5 kK on the map of Fig. 5 by computing maps with this error applied to the 22 MHz data in both senses. All the main features visible in Fig. 5 remain in both new maps. When we discuss the spectral features which we see in Fig. 5, we discuss only those which survive this test.

The effects of temperature scale errors are more difficult to assess. Once again, the large frequency separation is an asset. At the zenith (declination 48.8°) we have an independent determination of spectral index since we have not changed our data in any way at that declination. We estimate that the probable error there is 0.05, taking into account both systematic and random errors (amounting to

a 16% difference in the temperature ratio T_{22}/T_{408}), and we assign this error to the whole map. Further errors at other declinations depend on the validity of the assumption on which our calibration of the 22 MHz temperature scale is based, the constancy of the spectral index of the Galactic emission over the region 8^h to 16^h , -28° to 80° . This can only be tested with an extensive study of spectral index using data at a number of frequencies, a study beyond the scope of this paper. Note that we have assumed the constancy of the *differential* spectrum: we are assuming that the Galactic component of the emission has constant spectral index over this region, which includes the Galactic pole and lies mostly at latitudes higher than $\sim 20^\circ$. The *total* spectrum includes an extragalactic (presumably isotropic) component of emission, and the total

spectrum may still vary across this region, as it appears from Fig. 5 to do.

In the final analysis, the main value of our spectral index work is in the assessment of *differences* in spectral index between regions rather than in a precise determination of the spectral index of a given region. In this spirit, we make the following observations.

1. In general, the map in Fig. 5 shows few large scale variations. The mean index away from the Galactic plane is 2.47. Within this area (latitude greater than $\sim 10^\circ$) the mean index of extended regions varies from values of 2.41 in the area of synchrotron minimum ($10^{\text{h}}, 40^\circ$) to 2.54, near the position of Loop III, both with an rms variation of ~ 0.03 . On the Galactic plane, the flatter spectrum region coincident with the absorption trough at low longitudes is narrow in the latitude dimension. At all points on the Galactic plane it is notable that the spectral index is relatively constant over most of the broader synchrotron emission along the plane with no gradual decrease in spectral index as latitude decreases.
2. The outline of the North Polar Spur at higher latitudes can be seen in the spectral index map. An integration over the area of this arc shows its emission to have an index of 2.51, slightly steeper than its surroundings by ~ 0.03 .

6. Factors affecting the accuracy

6.1. Zero-level offsets

The offsets of the $T-T$ plots between 408 MHz and the final 22 MHz map are in the range ± 10 kK at 22 MHz. The mean of 11 offset values at intervals of 10° in declination from $+79^\circ$ to -21° is -5.1 kK with an rms deviation of 11.1 kK. This mean offset is of the same order as that derived for the $T-T$ plot of zenith data (see Fig. 1). From these data alone, however, it is not possible to decide the extent of the true offsets in either the 22 MHz or the 408 MHz data. The 408 MHz data is suspected of having offsets as large as 2 K (Reich & Reich 1988) and may also have a baselevel correction of 5 K. If the average spectral index between 22 and 408 MHz is 2.50, these values correspond to 2.8 kK and 7.2 kK at 22 MHz.

6.2. Effects of antenna properties on the data

In this section we examine the possible effects on our data of our imperfect knowledge of the properties of the antennas. The antennas used at 22 MHz and 408 MHz are of different types, and need to be discussed separately.

If emission received in the sidelobes made a significant contribution to antenna temperature, then errors would result. These would be especially significant in the map of

spectral index, because the sidelobe responses of the two very different antennas would receive emission from different parts of the sky. The greatest effect would occur in measurements of those parts of the sky where the brightness temperature is the lowest (around 9 hours, 30°) with emission from the bright Galactic plane being received in the far sidelobes of the antennas. As an example of such effects, Landecker & Wielebinski (1970), using the Parkes 64-m telescope at 150 MHz, found that about one third of the antenna temperature at the sky minimum arose from sidelobe contributions.

The response of the 22 MHz antenna is, in principle, completely calculable from the geometry of the array, and from the phasing and grading applied to the array elements. The angular size of the main beam proved to be very close to the calculated value. The net sidelobe solid angle should be zero, implying a beam efficiency of 1.0. Sidelobe responses, apart from their effects near strong sources, should not affect the measurement of the broad structure which is the focus of this paper. Measurements of the antenna response using the bright sources Cas A and Cyg A (Costain et al. 1969) bear out this expectation. The dynamic range of these measurements is about 30 dB, determined by the ratio of the flux density of Cyg A (29 100 Jy) to the confusion limit for the telescope (30 Jy). Sidelobes above this level were confined to the NS and EW planes (strictly a small circle EW, depending on the phasing in declination) and were alternately positive and negative, as expected, and close to the predicted amplitude. Sidelobe response fell below the detection limit within 10° of the main beam in the EW direction and below 1% within 18° of the main beam in the NS plane. These measurements verify our assertion that the performance of the telescope at the zenith is well understood (Cas A and Cyg A pass within 10° of the zenith at DRAO).

We are confident that the response of the antenna to the extended background was as predicted near the zenith because of the linear relationship between the 22 and 408 MHz brightness temperatures with the expected spectral index at that declination (48.8°). We know that the behaviour away from the zenith departed from the expected response for the extended emission features, but not for point sources. We tentatively attribute this to inadequately compensated mutual impedance effects between phased rows of dipoles in the array. At increasing zenith angles, these effects may have dominated the predicted response of individual dipoles above a reflecting screen.

The available measurements suggest, however, that the sidelobes of the complete telescope (as opposed to the individual groups of radiating elements) were still confined to the predicted regions, even at large zenith angles. If we assume that the sidelobe level was all positive and at the detection limit (-30 dB) in two 180° strips in the EW and NS directions, each equal in width to the main beam, then the beam efficiency would be 0.9, better than most

reflector antennas. However, this is very much a worst-case assumption, and it is probably safe to conclude that the beam efficiency was ≥ 0.95 . Furthermore, the largest sidelobes lie in the NS plane, and, when the main beam is measuring the coldest region of the sky, these sidelobes do not intersect the bright Galactic plane. We therefore feel justified in ignoring the effects of the sidelobe response of the 22 MHz telescope.

The 408 MHz data were not directly corrected for sidelobe contributions, but an indirect correction was applied (Haslam et al. 1982). The absolutely calibrated survey at 404 MHz made by Pauliny-Toth & Shakeshaft (1962) with a beam of about 7.5° was used to establish both the zero-level and the temperature scale of the 408 MHz survey data. Since the 404 MHz survey *was* corrected for sidelobe contributions, using it as a reference for the later survey roughly corrected those measurements for sidelobe contributions. The technique is valid in this case since the relationship between the measured antenna temperature and the sidelobe correction is, to a good approximation, linear. Checks of the effectiveness of this procedure were made subsequently by Lawson et al. (1987) and by Reich & Reich (1988) who convolved the 408 MHz data to the broad beams of horns and other low-sidelobe antennas used by Webster (1975) and Sironi (1974) to measure the Galactic emission at 408 MHz. In all cases the comparisons were satisfactory, indicating that sidelobe effects had been effectively removed from the 408 MHz data.

7. Discussion

7.1. Components of extended Galactic emission

Beuermann et al. (1985) have used the 408 MHz all-sky survey (Haslam et al. 1982) to produce a three-dimensional model of the Galactic radio emission using an unfolding procedure. In this model the Galaxy consists of a thick non-thermal radio disk in which a thin disk is embedded. The thick disk exhibits spiral structure, has an equivalent width of ~ 3.6 kpc at the solar radius and accounts for $\sim 90\%$ of the diffuse 408 MHz emission. Emission extends to at least 15 kpc from the Galactic centre, at which radius the thick disk has an equivalent width near 6 kpc. The *thin* disk, by comparison, appears in the model as a mixture of thermal and non-thermal emission also with spiral structure, but with an equivalent width of ~ 370 pc, similar to that of the HI disk and of the distribution of HII regions in the inner Galaxy.

Our comparison of the 22 MHz and 408 MHz maps shows a remarkable constancy of spectral index in the extended emission corresponding to the thick disk component over our full range of longitudes from $\sim 0^\circ$ to $\sim 240^\circ$. The principal departures from this general tendency are (i) the slightly flatter spectral index in a broad area in the region of minimum Galactic emission at high latitudes toward the longitude of the Galactic anticentre and (ii) the

somewhat steeper indices near Loop III and the outer rim of the NPS. In a similar comparison of the 408 MHz map with a map of 1420 MHz emission, Reich & Reich (1988) also note these general features. However, we see no indication in the lower frequency range for the steeper spectra seen by Reich & Reich in regions on the plane both near the Galactic centre and near longitude 130° . This suggests that any steepening of the spectra in these regions must be a higher frequency phenomenon with spectral curvature above 408 MHz.

Details of the spectral index variations associated with the loops of emission also differ in the two frequency ranges. Figure 5 shows a slightly steeper index (by ~ 0.03) for a substantial part of the arc forming the outer edge of the NPS. This contrasts with the 408 – 1420 MHz comparison (Reich & Reich 1988) which shows a steeper index in a relatively broad arc on the part of the NPS closest to the Galactic plane. Neither study indicates a difference between the spectral index of emission within the loop of the NPS and that outside the loop. The NPS has variously been considered as a nearby, very old supernova remnant (e.g. Salter 1983) and as a local magnetic “bubble” (Heiles 1998).

7.2. Absorption at lower longitudes

We have noted that at longitudes less than $\sim 40^\circ$ there exists a continuous trough of absorption along the Galactic plane. We illustrate this in Fig. 6 which shows a map of the “quasi optical depth” at 22 MHz calculated from a comparison with the 408 MHz map on the assumption that the absorption is due entirely to cool ionized gas on the near side of the emission. (We define quasi optical depth, τ' , by the relation $\tau' = \ln(T_{408}(408/22)^{\beta'}/T_{22})$, where β' is the mean spectral index of the emission off the Galactic plane). This represents an underestimate of the true optical depth of the absorbing gas since (i) a proportion of the non-thermal emission will be on the near side of some absorption and, (ii) the kinetic temperature of the thermal gas will lessen the apparent depth of the absorption. A more accurate estimate of the true optical depth would require a modelling of the intermixed emission and absorption components which is beyond the scope of this paper. Nonetheless, it is obvious from Fig. 6 that the full angular width of the absorbing region is less than 3° which, at an assumed mean distance of 4 kpc, corresponds to a thickness of less than 250 pc. Thus, it is apparent that the absorption corresponds to the “thin disk component” of emission identified by Beuermann et al. (1985) as comprising the known disks of HII regions, diffuse thermal continuum emission, diffuse recombination line emission and the distribution of atomic hydrogen.

The extended absorption in the plane in the region of Cygnus between longitudes 70° and 90° is also shown in Fig. 6. Note that the region appears at least twice as

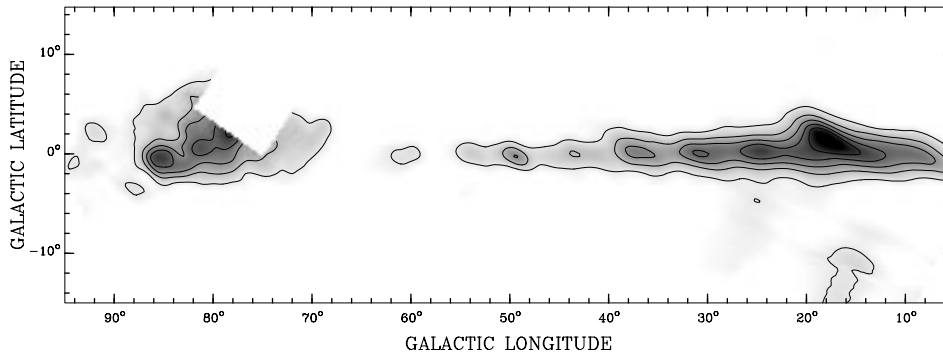


Fig. 6. The “quasi optical depth” at 22 MHz along the Galactic plane in the first quadrant, from a comparison of the 408 MHz and 22 MHz emissions, assuming all absorbing (thermal) gas is on the near side of the background synchrotron emission. Contours are at optical depths of 0.4, 0.8, 1.2, 1.6 and 2.0

Table 3. Synchrotron emissivities in the directions of H II regions

Galactic Coordinates	Region	Distance parsecs	Foreground emission kK	Emissivity K/pc
6.3 + 23.5	Sh 27	170 ^a	27.0	159
85.5 – 1.0	Sh 117	800 ^b	17.4	21.8
99.3 + 3.7	Sh 131	860 ^c	37.4	43.5
118.5 + 6.0	NGC 7822	840 ^c	30.1	35.8
134.8 + 0.9	IC 1805	2200 ^c	46.0	20.9
160.1 – 12.3	Sh 220	400 ^c	23.9	59.8
195.1 – 12.0	Sh 264	400 ^c	20.4	51.0
202.9 + 2.2	Sh 273	800 ^d	23.1	28.9

^a Georgelin et al. (1973)

^b Georgelin (1975)

^c Humphreys (1978)

^d Turner (1976).

Note: The electron temperature in the H II regions is assumed to be 6000 K.

extensive in latitude as the continuous trough, probably because much of the absorbing gas is at distances of 1 kpc or less.

7.3. Non-thermal emissivities in the plane

Several of the discrete H II regions which appear in absorption at 22 MHz and which are listed in Table 2 can be used to estimate the emissivity of local synchrotron emission. We have calculated the emissivities for eight H II regions at well-determined distances, which are sufficiently extended compared to the observing beam to ensure that only thermal radiation from the ionized gas and foreground non-thermal radiation contribute to the measured emission. An assumed contribution from the opaque ionized gas of 6000 K was subtracted from the brightness temperature in the depression and the result divided by the distance to the H II region. The values of emissivity are presented in Table 3.

In the longitude range 85° to 205°, six H II regions are at distances from 400 – 900 pc and the values of 22 MHz

emissivity¹ range from 21 Kpc⁻¹ to 60 Kpc⁻¹ with a mean of 40.1 Kpc⁻¹. Excluding two H II regions, Sh220 and Sh264, which are more than 10° off the plane, but including IC 1805, at a distance of 2.2 kpc, we find a mean emissivity of 30.2 Kpc⁻¹ with an rms of 9.6 Kpc⁻¹. These emissivities are comparable with similarly derived emissivities tabulated (at 10 MHz) by Rockstroh & Webber (1978). In addition, our value in the direction of IC 1805, 20.9 Kpc⁻¹, is close to the value of 18 Kpc⁻¹ obtained by Roger (1969) using a detailed modelling of 22 and 38 MHz data for the IC 1805–IC 1848 complex.

However, there is a problem reconciling a mean value of local emissivity of 30 Kpc⁻¹ with the model of Galactic emission of Beuermann et al. (1985) which assumes a lesser value of 15 Kpc⁻¹ (11 Kkpc⁻¹ at 408 MHz) at the solar radius. If we take the value of the brightness temperature at the Galactic poles (27 kK), subtract an extragalactic component of 6 kK (Lawson et al. 1987) and divide by the model’s half-equivalent-width of 1.8 kpc, we derive a mid-plane emissivity of only 11.7 Kpc⁻¹, almost a

¹ A volume emissivity per unit line-of-sight of 1 Kpc⁻¹ is equal to $4.93 \cdot 10^{-42} \text{ W m}^{-3} \text{ Hz}^{-1} \text{ sr}^{-1}$ at 22 MHz.

factor of 3 less than our measured mean value. To reconcile our measurement with the model, one or more of the following must apply: *(i)* our measured local mean emissivity is greater than the typical value at the solar radius; *(ii)* the equivalent width of the “thick-disk” component is locally less than the model predicts; *(iii)* the extragalactic component of the polar emission is less than is estimated from extrapolations of extragalactic source counts at higher frequencies; and/or *(iv)* a zero-level correction should be added to the 22 MHz brightness temperatures. With regard to the extragalactic component of emission, we note that estimates are usually derived from source count (“log $N - \log S$ ”) analyses at frequencies above 150 MHz (e.g. Lawson 1987), extrapolated with an assumed spectral index $\beta \approx 2.75$. Analyses of source counts at substantially lower frequencies are needed for accurate estimates of the extragalactic component. We noted in Sect. 6.1 the possibility of a zero-level correction as indicated by $T-T$ plot comparisons with 408 MHz data. In this regard, it is interesting to note that very low resolution measurements with scaled antennas at several low frequencies (Bridle 1967) predicted a brightness temperature at 22 MHz in the area of the North Galactic Pole 4 kK higher than our value. This is of the same magnitude and sense as the offset suggested by the $T-T$ plot analysis.

We note the unusually high emissivity derived for the direction toward ζ -Oph (Sh27), a relatively nearby complex some 23° above the plane at the longitude of $\sim 6^\circ$. Emission from this direction may include components from the North Polar Spur and from a minor spur that is most prominent near $l = 6^\circ$, $b = 14^\circ$, both of which may be foreground features. Also, it is possible that this somewhat diffuse region is not completely opaque at 22 MHz, in which case an unknown amount of background emission may contribute a spurious component to the emissivity.

Acknowledgements. We are indebted to several colleagues for their assistance in collecting and processing the observational data, and we particularly thank J.D. Lacey, J.H. Dawson and D.I. Stewart. We are also grateful to Dr. J.A. Galt for his encouragement at various stages of this project.

References

- Alvarez H., Aparici J., May J., Olmos F., 1997, A&AS 124, 315
 Beuermann K., Kanbach G., Berkhuisen E.M., 1985, A&A 153, 17
 Bridle A.H., 1967, MNRAS 136, 219
 Caswell J.L., 1976, MNRAS 177, 601
 Costain C.H., Lacey J.D., Roger R.S., 1969, IEEE Trans-AP 17, 162
 Ellis G.R.A., 1982, Aust. J. Phys. 35, 91
 Georgelin Y.M., 1975, thèse de doctorat, Université de Provence
 Georgelin Y.M., Georgelin Y.P., Roux S., 1973, A&A 25, 337
 Hamilton P.A., Haynes R.F., 1969, Aust. J. Phys. 22, 839
 Haslam C.G.T., Salter C.J., Stoffel H., Wilson W.E., 1982, AAS 47, 1
 Heiles C., 1998, The Magnetic Field near the Local Bubble. In: Breitschwerdt D., Freyberg M.J., Trümper J. (eds.) Proc. IAU Coll. 166, The Local Bubble and Beyond. Springer-Verlag, Lecture Notes in Physics, Vol. 506
 Humphreys R.M., 1978, ApJS 38, 309
 Landecker T.L., Vaneldik J.F., Dewdney P.E., Routledge D., 1987, AJ 94, 111
 Landecker T.L., Wielebinski R., 1970, Aust. J. Phys. Suppl. 16, 1
 Lawson K.D., Mayer C.J., Osborne J.L., Parkinson M.L., 1987, MNRAS 225, 307
 Milogradov-Turin J., Smith F.G., 1973, MNRAS 161, 269
 Pauliny-Toth I.I.K., Shakeshaft J.R., 1962, MNRAS 124, 61
 Pineault S., Landecker T.L., Swerdlyk C.M., Reich W., 1997, AA 324, 1152
 Reich P., Reich W., 1988, A&AS 74, 7
 Rockstroh J.M., Webber W.R., 1978, ApJ 224, 677
 Roger R.S., 1969, ApJ 155, 831
 Roger R.S., Bridle A.H., Costain C.H., 1973, AJ 78, 1030
 Roger R.S., Costain C.H., 1976, AA 51, 151
 Roger R.S., Costain C.H., Lacey J.D., 1969, AJ 74, 366
 Roger R.S., Costain C.H., Stewart D.I., 1986, AAS 65, 485
 Salter C.J., 1983, Bull. Astr. Soc. India 11, 1
 Sironi G., 1974, MNRAS 166, 345
 Turner D.G., 1976, ApJ 210, 65
 Turtle A.J., Baldwin J.E., 1962, MNRAS 124, 459
 Webster A.S., 1975, MNRAS 166, 355